Paradoxical motion of a single Brownian particle: Absolute negative mobility

Ralf Eichhorn and Peter Reimann
Fakulät für Physik, Universität Bielefeld, D-33615 Bielefeld, Germany

Peter Hänggi
Theoretische Physik I, Institut für Physik, Universität Augsburg, D-86135 Augsburg, Germany
(Received 19 August 2002; published 26 December 2002)

We consider a single, classical Brownian particle in a spatially symmetric periodic system far from thermal equilibrium, which can be readily realized experimentally. Upon application of an external static force F, the average particle velocity is negative for $F>0$ and positive for $F<0$ (absolute negative mobility). The various physical mechanisms responsible for such a paradoxical effect are identified, leading to analytical approximations that are in good agreement with numerical simulations.

I. INTRODUCTION

When a system at rest is perturbed by a static force, we expect that it responds by moving into the direction of that force. The rather surprising opposite behavior in the form of a permanent average motion against a (not too large) static force of any direction is called *absolute negative mobility* (ANM). If the unperturbed system is at thermal equilibrium, then ANM is impossible since it could be exploited to construct a *perpetuum mobile* of the second kind. Familiar to everyone, but rather complex nonequilibrium systems that do exhibit ANM are donkeys [1].

Much simpler and better controlled nonequilibrium systems in which ANM has been experimentally and theoretically studied under the label of *absolute negative conductance or resistance* are different kinds of semiconductor devices [2–12], photovoltaic effects in ruby crystals [13–16], tunnel junctions between superconductors with unequal energy gaps [17–19], and a simplified theoretical model for certain ionized gas mixtures [20–22]. In all these cases, the physical roots for the appearance of ANM are genuine *quantum mechanical* effects that do not survive in the limit towards a classical description.

A second class of nonequilibrium systems exhibiting ANM consists of various theoretical models of *interacting* Brownian particles [23–27]. In this case, the underlying physical mechanisms are of purely classical character, but now *collective effects* are an indispensable ingredient for the manifestation of ANM. While in most of these studies, the main focus is on systems with a large number of interacting particles, a toy model that requires as few as three particles has been put forward in Ref. [1]. Yet, a further reduction to one single particle exhibiting ANM was commonly assumed to be impossible among those practitioners.

With our present paper we continue and provide the details of our brief account [28] on the existence of ANM in purely classical, single-particle models that can be readily realized experimentally. An independent, closely related, but complementary investigation has been recently published in Ref. [29]. While the effect of ANM is the same, the proposed models therein are completely different from ours and may not be so straightforward to realize in an experiment.

The common denominator of the different models that we will treat in the present work is their spatial periodicity and inversion symmetry. Furthermore, upon application of an external static "load" force F, these models respond with an average particle current that always runs into the direction *opposite* to that of F (provided F is not too large in modulus). Especially, no average current arises when $F=0$ due to the spatial symmetry. In other words, the current-load curve exhibits a passage through the origin with a negative slope as its most prominent feature, which, in fact, constitutes the defining property of ANM.

In contrast to ANM, the so-called ratchet effect [30–34] is characterized by an average particle current that is nonzero for $F=0$ and does not change its direction within an entire neighborhood of $F=0$. This effect thus inevitably involves some kind of asymmetry (for $F=0$). Moreover, the response of a ratchet system to an applied load force F results usually in a change of the current in accordance with the sign of that force, i.e. the current-load curve passes through $F=0$ not only with a finite offset but also with a positive slope. The latter property, in fact, holds true for all existing ratchet systems we are presently aware of [33]. There is in principle no reason, however, that this has to be always so, and counterexamples can actually be constructed by straightforward asymmetric modifications of our present models.

Put differently, the salient difference between the ratchet effect and ANM is as follows: In an equilibrium system, the second law of thermodynamics forces the current-load curve to pass through the origin with a nonnegative slope. In a ratchet system, the main nonequilibrium effect is a vertical shift of that curve, while ANM exploits the disequilibrium to turn the slope negative without a concomitant offset.

Also note that ANM is distinct from so-called *differential negative mobility* (or resistance) [35–39] which is typified by a negative slope of the current-load curve *away* from the origin $F=0$. It characterizes a current that is oriented in the direction of the bias but decreases with increasing F. In contrast to ANM or the ratchet effect, differential negative mobility can also occur in equilibrium systems if subjected to an external static bias [37].

The present paper is organized as follows: In Sec. II, we introduce our model and the basic quantity of interest,
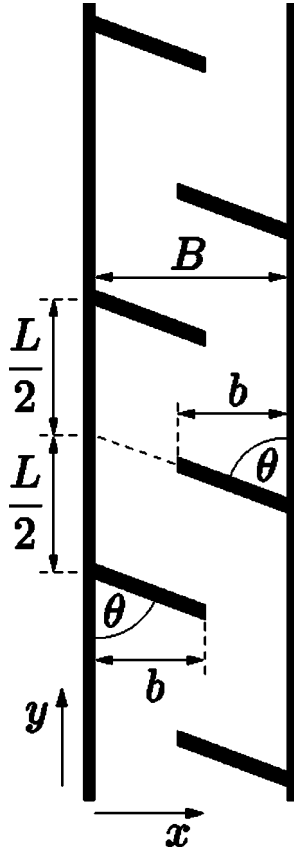
$$\eta\dot{x}(t) = -\partial_x V(x(t), y(t)) + \xi_x(t), \tag{1a}$$

$$\eta\dot{y}(t) = -\partial_y V(x(t), y(t)) + \zeta_y(t) + F. \tag{1b}$$

In comparison to the usual Newtonian equation, the inertia terms $m\ddot{x}(t)$ and $m\ddot{y}(t)$ are omitted, since in typical experimental systems these inertial effects are negligibly small. In Eq. (1), η denotes the viscous friction coefficient, $V(x,y)$ is the hard-wall potential from Fig. 1, and F is a static "tilting force." Further, the thermal fluctuations are modeled by unbiased Gaussian white noise $\xi_x(t)$ with correlations

$$\langle \xi_x(t)\xi_x(s)\rangle = 2\eta k_B T \,\delta(t-s), \tag{2}$$

where k_B denotes Boltzmann's constant, T the temperature, and $\langle\cdot\rangle$ indicates the ensemble average over many independent realizations in Eq. (1).

Aiming at nonequilibrium effects, $\zeta_y(t)$ cannot be simply a second thermal white noise, but rather must include appropriate time-dependent forces (with zero mean) to drive the system out of thermal equilibrium. From a theoretical viewpoint, the simplest such source of disequilibrium is a *symmetric* dichotomous noise that switches randomly at a rate γ between two states $\pm A$. The respective distribution of sojourn times then reads

$$\rho(\tau) = \gamma e^{-\gamma\tau} \quad [\text{dichotomous noise } \zeta_y(t)]. \tag{3}$$

Another choice for $\zeta_y(t)$ (which we will not pursue in detail in this paper) would be, e.g., colored Gaussian noise (which does not satisfy a generalized fluctuation-dissipation theorem of the second kind [40]). While conceptually appealing due to their simplicity, such models for $\zeta_y(t)$ without a thermal noise component are hard to realize experimentally.

One possible experimental realization we have in mind is based on the techniques used in Refs. [41–55]. Micrometer-sized beads in a dilute colloidal suspension at room temperature serve as practically noninteracting Brownian particles. The potential landscape of Fig. 1 (or one of the generalizations introduced in Sec. IV) can be built by means of light forces [43,47,52–54,56,57], electric fields [42,43,45,46,49,55] or morphologically via lithographic etching methods [41,51]. The external forces can be realized, e.g., by electric [41,51] or magnetic [50] fields or by making use of gravitation. Indeed, an experimental realization of our model along these lines is currently being constructed by Bechinger and co-workers.

A realistic choice for the noise source $\zeta_y(t)$ in such an experiment is composed of a symmetric periodic force $f(t)$ that switches between $\pm A$ with period 2τ and, in addition, another thermal white noise $\xi_{th}(t)$ like $\xi_x(t)$ in Eq. (2) but statistically independent, i.e., $\langle \xi_x(t)\xi_{th}(s)\rangle = 0$ for all t,s,

$$\zeta_y(t) = \xi_{th}(t) + f(t). \tag{4}$$

Our central observable is the mean particle current through the corridor

$$\langle\dot{y}\rangle := \left\langle \lim_{t\to\infty} \frac{y(t)-y(t_0)}{t-t_0} \right\rangle. \tag{5}$$

FIG. 1. Hard-wall potential $V(x,y)$, defined as zero in the white regions and infinity in the black regions. The particle moves inside this corridor of width B, the white regions outside are of no interest. The symmetrically and periodically (with period L) arranged obstacles are characterized by the parameters b and θ. Note that $b > B/2$.

namely, the average particle current. Additionally, a formal definition of ANM is given. Section III is devoted to a detailed analysis of the physical mechanisms that are responsible for the occurrence of ANM in our model under periodic nonequilibrium perturbations. Based on an intuitive understanding of these mechanisms at work, we develop a simple theory that is in good agreement with numerical simulations. In Sec. IV, various generalizations of the original model are introduced and discussed. Finally, the summary and discussion of our findings are presented in Sec. V.

II. MODEL

We consider a Brownian particle in a two-dimensional hard-wall "corridor" with obstacles that are arranged *periodically* and *symmetrically under spatial inversion*, rendering a straightforward passing of the "corridor" impossible, as in Fig. 1. The particle is subjected to both random thermal fluctuations and externally applied forces acting along the "corridor." Taking the "corridor axis" as the y direction of our coordinate system, the dynamical behavior of the particle is modeled by the coupled two-dimensional overdamped Langevin equation,
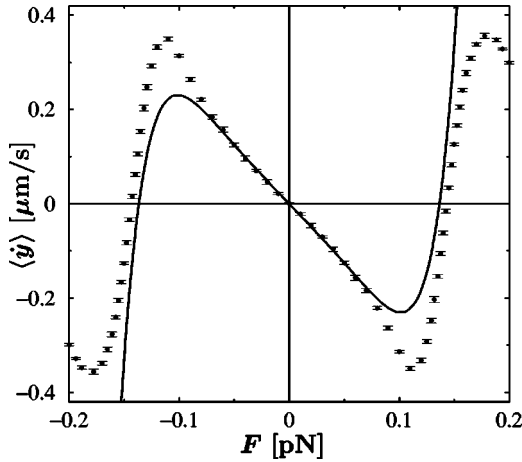
FIG. 2. Current-load characteristics (or load curve) for Eq. (1) with the potential $V(x,y)$ of Fig. 1, the periodic nonequilibrium noise source (4), and parameter values $L=4$ μm, $B=3$ μm, $b=1.2$ μm, $\theta=70°$, $T=293$ K, $A=0.2$ pN, $\tau=1$ s [hence $A1$ μm $\approx 50k_B T$ and $\tau \approx 5\tau_L$ for $F_{tot}=0.2$ pN, where $\tau_L=\eta L/F_{tot}$ is the mean time the particle needs to cover a period L by free drift; see Eq. (16)]. Dots with error bars represent numerical simulations of Eq. (1). Solid lines represent analytic approximation (10) with Eqs. (12) and (13). The Brownian particle is assumed as spherical with radius $r=0.5$ μm and as subjected to Stokes friction $\eta=6\pi\nu r$, where ν is the viscosity of water. The finite particle radius r has been approximately accounted for by replacing B by $B-2r$ in Eq. (12). The choice of the above parameter values has been made with the experimental realization described above Eq. (4) in mind.

Due to the long-time limit $t\to\infty$, the right-hand side of Eq. (5) becomes independent of the initial conditions t_0 and $y(t_0)$. Moreover, due to self-averaging (or ergodicity) reasons, the ensemble average may be omitted as well [33], i.e., we may recast Eq. (5) as

$$\langle \dot{y} \rangle = \lim_{t\to\infty} \frac{y(t)}{t}. \tag{6}$$

The current-load characteristics (or load curve) that displays the current (5) as a function of the static load F (cf. Fig. 2) exhibits an odd symmetry with respect to F due to the y symmetry of the potential landscape in Fig. 1 and of the nonequilibrium driving $\zeta_y(t)$: $\langle\dot{y}\rangle \to -\langle\dot{y}\rangle$ for $F\to-F$. In particular, we have

$$\langle \dot{y} \rangle = 0 \text{ for } F=0. \tag{7}$$

ANM is characterized by a current (5) that runs (at least for sufficiently small F) *opposite* to F, independent of whether F is positive or negative. Formally, ANM is thus defined as

$$\left. \frac{d\langle \dot{y} \rangle}{dF} \right|_{F=0} < 0, \tag{8}$$

together with property (7). For large values of the bias F, the current (5) will in general again adopt the direction of F; this regime, however, is not at the focus of our present work.

In an equilibrium system (1), the current (5) always runs into the direction of the static force F, because ANM is forbidden at thermal equilibrium. If this was not so, we readily could construct a *perpetuum mobile* of the second kind: Under a periodically switching external load $\pm F$, the particle would (on average) cyclically move back and forth, thereby performing useful work *against* this bias. Consequently, $d\langle\dot{y}\rangle/dF|_{F=0}>0$ in thermal equilibrium. For continuity reasons, $d\langle\dot{y}\rangle/dF|_{F=0}$ still remains positive for small deviations from equilibrium, implying that model (1) cannot exhibit ANM close to thermal equilibrium. Turning to situations far away from thermal equilibrium, however, permanent motion opposite to the external force is no longer ruled out *a priori*. In fact, ANM occurs [28] in our system (1) for sufficiently strong nonequilibrium driving (4), as depicted with Fig. 2. The physical origin for the occurrence of ANM in Eq. (1), as well as a theoretical description of this phenomenon, will be the subject of the following sections.

III. ANM FOR PERIODIC DRIVING

Out of the various possibilities for the nonequilibrium noise source $\zeta_y(t)$ mentioned in the preceding section, let us first focus on the case that may be understood most readily, the combination of thermal fluctuations with deterministic periodic driving, as given in Eq. (4).

We can adopt the following simplified picture of our model (1). The particle moves in the potential landscape of Fig. 1 under the influence of thermal fluctuations and, in addition, is subjected to the *total* external force

$$F_{tot} := F \pm A, \tag{9}$$

acting in the y direction along the corridor. The total force (9) switches periodically between $F+A$ and $F-A$ with period 2τ and average value F.

In each of the two states $F\pm A$ of Eq. (9) with sojourn time τ, the particle travels on average a distance $\Delta y(\tau,F_{tot})$ along the corridor. The net particle current (5) thus follows as

$$\langle \dot{y} \rangle = \frac{\Delta y(\tau,A+F) - \Delta y(\tau,A-F)}{2\tau}. \tag{10}$$

For later convenience, we have written $-\Delta y(\tau,A-F)$ instead of $+\Delta y(\tau,F-A)$ for the second term in the numerator, thereby exploiting the odd y symmetry of our system (1). Due to this symmetry, we furthermore can restrict ourselves without loss of generality to $A>0$ and $F\geq0$ in the following.

As already mentioned at the end of the preceding section, ANM cannot occur in Eq. (1) close to thermal equilibrium, i.e., for small A or small τ. This is a consequence of linear response theory for stochastic processes at high frequency [58]. However, simply making A large is not sufficient either to create ANM. If $A<F$, the total force (9) points permanently into the direction of F, and the average particle current (5) thus adopts the same orientation as the static load, even if we are far away from thermal equilibrium. For ANM, we thus have to focus at least on the regime $A>F$. Then, the
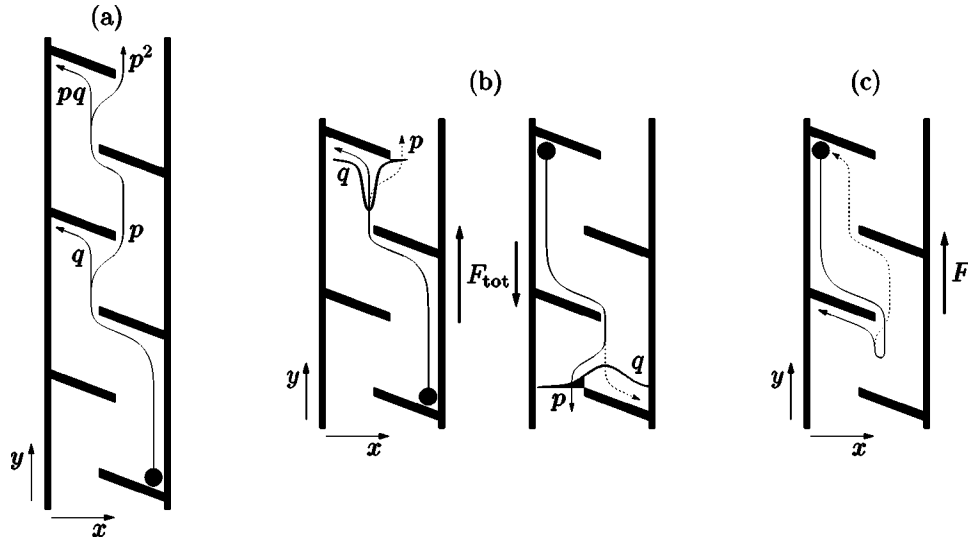
FIG. 3. (a) Typical traveling routes of the particle for $F_{\text{tot}} > 0$ together with their probabilities ($q := 1 - p$). (b) Traveling routes for a large positive force $F_{\text{tot}} = F + A$ (left) and a small negative force $F_{\text{tot}} = F - A$ (right). For the large force, the traveling speed v_y is large and the particle has only a little time to thermally diffuse along the x direction, as indicated by a narrow (approximately) Gaussian profile. The particle thus typically ends up by being trapped, and the probability p for avoiding a trap is very small. For the small force, the drift velocity v_y is smaller. Consequently, the available time for diffusive "broadening" is larger (broader Gaussian profile) resulting in a noticeable probability p of avoiding the trap. The respective values of p are indicated by the filled parts of the Gaussian profiles. The dashed paths do not contribute to ANM. See also the main text. (c) Typical traveling routes for fast nonequilibrium driving with sojourn times τ just smaller than $3 \eta L / 2 (A - |F|)$ [see also Eq. (14)]. Before the particle can cover the "basic distance" $3L/2$ but after it has traveled at least one period L, the external force F_{tot} switches from $F - A < 0$ to $F + A > 0$, indicated by the turning point of the particle route. The solid path showing immediate trapping after reversal of the force is at the origin of ANM. The dashed path yields no net motion. Both routes occur with an approximate probability of 1/2.

two states $F \pm A$ of the total force (9) are of different sign, and the current (10) constitutes the net result from the different average distances the particle travels in the opposite directions.

The above conditions imposed on A and F imply that $A + F > A - F$. In view of Eq. (10), we can thus infer that a current (5) opposite to the static force F, and therefore ANM, may emerge only if statistical paths dominate where the mean traveling distance $\Delta y(\tau, F_{\text{tot}})$ is *smaller* for *larger* forces F_{tot}.

A. Moderately fast driving

The system parameters in Fig. 2, in particular the characteristic time scale τ of Eq. (4), are chosen such that the nonequilibrium noise source operates in the regime of rather high frequency $1/(2\tau)$, i.e., the particle can travel at most a few periods L by free drift within the time τ. The physical mechanism leading to ANM for this "moderately fast" driving can be understood as follows. Consider a particle being located in one of the "corners" between the right "corridor wall" and any of the adjacent obstacles [see Fig. 3(a)] at the beginning of the time interval τ with constant $F_{\text{tot}} > 0$. Due to this external force, a drift with velocity

$$v_y := F_{\text{tot}} / \eta \tag{11}$$

in the positive y direction is induced, additional to the diffusive motion stemming from the thermal environment. If the ambient thermal noise is not too strong, and hence the diffu-

sion proceeds not too fast, the particle in Fig. 3(a) first closely follows the right "corridor wall," not being hindered by the neighboring obstacle to the left. It then hits the next obstacle (at the right corridor wall) and "slides down on the back" of that obstacle until it "falls off" to perform a "free fall" in the positive y direction. Because the lateral extension of the obstacles b exceeds half the corridor width $B/2$, the particle then hits with a high probability q, the next obstacle on its way and ends up being trapped in the corresponding corner between that obstacle and the left corridor wall. In order to avoid this trap, the particle must thermally diffuse at least over a distance $b - (B - b) = 2b - B$ in the positive x direction during its free fall in the y direction. With increasing total force (9), "free traveling speed" (11) increases, implying that the available time and therefore the probability $p := 1 - q$ of such a diffusive displacement decreases, see Fig. 3(b). Consequently, the particle travels on average a *shorter* distance along the y axis during the time τ for *larger* forces F_{tot}. As discussed above, see below Eq. (10), it is this very mechanism that implies the occurrence of ANM.

In order to quantify these qualitative findings, we calculate the average traveling distance $\Delta y(\tau, F_{\text{tot}})$ for $F_{\text{tot}} > 0$; the current (5) then follows according to Eq. (10). To this end, we start by approximating the above mentioned probability p of avoiding a trap. After drifting for a time t along the y axis with speed v_y from Eq. (11), the thermal diffusion along the x axis is approximately captured (for not too large t) by a Gaussian distribution with variance $2Dt$. For a particle that closely passes by the leftmost edge of an obstacle

attached to the right corridor wall (for $F_{\text{tot}} > 0$), the probability p is determined by this part of the Gaussian distribution which lies beyond the rightmost edge of the next "trapping" obstacle [see Fig. 3(b)]. By use of Einstein's relation $D = k_{\text{B}}T/\eta$ and observing that neighboring obstacles have an overlap $b - (B - b) = 2b - B$ (in x direction) and an approximate distance $L/2$ (in y direction), we obtain

$$p(F_{\text{tot}}) = \frac{1}{2} \ \text{erfc}\left(\frac{2b - B}{\sqrt{2Lk_{\text{B}}T}} \sqrt{F_{\text{tot}}} \right) \quad \text{for} \ \ F_{\text{tot}} > 0, \quad (12)$$

where $\text{erfc}(x) := 2\pi^{-1/2}\int_x^\infty e^{-u^2} du$ is the complementary error function. With probability p, a particle thus covers in addition to the "basic distance" of approximately $3L/2$ from one of the (right) corners up to the first "trapping" obstacle another period L [see Fig. 3(a)]. It then avoids the second trap on its way with approximately the same (relative) probability p as in Eq. (12), i.e., a second period L is covered with (absolute) probability p^2, etc. [see Fig. 3(a)]. If the maximal traveling distance (avoiding all traps) is of the form $(3/2 + N)L$ with $N \in \mathbb{N}$, the average traveling distance $\Delta y(\tau, F_{\text{tot}})$ thus follows as $L[3/2 + p + p^2 + \cdots + p^N]$. Neglecting the fact that the free traveling speed v_y is slightly reduced when the particle "slides down on the back" of an obstacle, we obtain $(3/2 + N)L = v_y\tau$; hence, in virtue of Eq. (11), we find

$$\Delta y(\tau, F_{\text{tot}}) = L\left\{ \frac{1}{2} + \frac{1 - [p(F_{\text{tot}})]^{F_{\text{tot}}\tau/(\eta L) - 1/2}}{1 - p(F_{\text{tot}})} \right\}. \quad (13)$$

This expression can also be used as a decent interpolation even if $v_y\tau$ does not precisely equal $(3/2 + N)L$.

With the average traveling distance (13), current (5) is finally obtained from Eq. (10). As can be inferred from Fig. 2, the agreement of this analytic prediction with the simulations is remarkably good despite the various approximations underlying our theoretical estimates in Eqs. (12) and (13):

(i) The thermal noise $\xi_{\text{th}}(t)$ from Eq. (4) which couples to the y component of Eq. (1), has been neglected, thereby tacitly assuming that corresponding corrections to Eqs. (12) and (13) are small.

(ii) In order to obtain Eq. (12), we have assumed that the probability distribution resulting from the lateral diffusion of the particle during its free fall possesses a Gaussian shape, and we have thus neglected effects of the corridor walls.

(iii) The drift distance in the y direction between subsequent obstacles has been supposed to equal $L/2$, which is justified as long as $\theta < 90°$ is not too small, see in Fig. 1. In fact, for very small θ, neighboring obstacles have an overlap in the y direction. Then the probability p for avoiding a trap becomes exactly zero, independent of F_{tot}, implying that the crucial mechanism for ANM cannot occur at all. For $\theta = 90°$, ANM is found to disappear as well in numerical simulations of Eq. (1).

(iv) We have used the assumption that the particle first closely follows the (right) corridor wall up to the next obstacle attached to this wall, see Fig. 3(a). This approximation becomes doubtful for $k_{\text{B}}T/F_{\text{tot}} > (B - b)^2/L$ because the par-

ticle can then get trapped with considerable probability already by the very first obstacle (to the left) due to lateral diffusion away from the corridor wall.

While these conditions (i)–(iv) basically refer to the geometrical properties of the corridor, the derivation of our theoretical results, in particular the result in Eq. (13), is moreover based on further assumptions that involve the time scale τ of the nonequilibrium force (4):

(v) The expression (13) is only valid if the particle covers at least the "basic distance" $3L/2$ during the time τ, i.e., if $v_y\tau = F_{\text{tot}}\tau/\eta > 3L/2$.

(vi) We have completely neglected the possibility that a trapped particle may escape from its trap due to the ambient thermal noise. This is only justified as long as τ is much smaller than the mean escape time $\tau_{\text{esc}}(F_{\text{tot}})$ out of a trap. In passing we note that under such an assumption the particle mostly lingers in one of the "sticky corners" before a switch of F_{tot} occurs; this is consistent with our approach to take these corners as initial positions for the motion of the particle within a time interval τ.

The latter two requirements are fulfilled for both forces $F_{\text{tot}} = F \pm A$ and the sojourn time τ contributing in Eq. (10) if they hold for the *smaller* force $A - F$, i.e., if

$$\frac{3\eta L}{2(A - F)} < \tau \ll \tau_{\text{esc}}(A - F), \quad (14)$$

where $A > 0$ and $F \geq 0$ have been tacitly assumed. This relation defines our "moderately fast" driving regime in quantitative terms. For intermediate $\tau \approx \tau_{\text{esc}}$ and large $\tau \gg \tau_{\text{esc}}$ ANM subsists, whereas for smaller driving intervals τ ANM eventually disappears. These latter driving regimes will be discussed in detail in the following sections.

B. Fast driving: Bursting and disappearance of ANM

For shorter half periods $\tau < 3\eta L/2(A - F)$, ANM is found to vanish in numerical simulations of Eq. (1). Before this disappearance occurs, we observe—much to our own surprise—an *enhancement* of ANM, see in Fig. 4. This remarkable feature is rooted in a completely different mechanism, illustrated in Fig. 3(c): Suppose, we are just beyond the driving-regime characterized in Eq. (14), i.e., the sojourn time τ with constant $F_{\text{tot}} = F - A$ (the small force) is too short to cover the "basic distance" $3L/2$ with the "free traveling speed" (11), but still sufficiently large to advance at least by one period L. Then, the external forcing switches to the state $F_{\text{tot}} = F + A$ (the large force) during the free fall of the particle towards the first trap, see Fig. 3(c). Drifting now into the opposite direction, the particle either gets trapped by the obstacle it just has passed by, or else, it avoids this trap to finally end up (with high probability) in its original starting corner. In the latter case, no net motion has occurred, whereas in the former case a period L has been covered into the direction *opposite* to the static force F, i.e., we again find ANM. The respective probability for getting trapped is close to $1/2$, and therefore much larger than the typical probability p for avoiding a trap in the moderately fast-driving mecha-
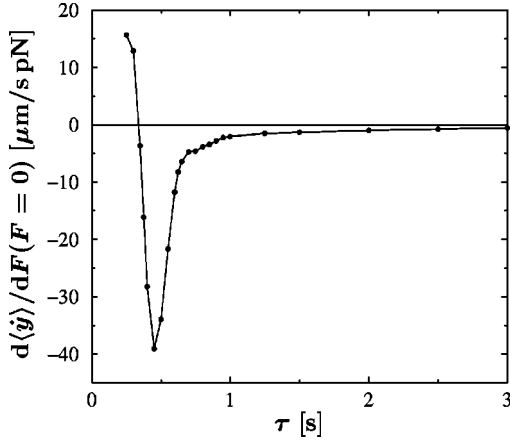
FIG. 4. Enhancement of ANM for fast driving. Shown as dots is the *slope* of the current-load curve at $F=0$ as it depends on the characteristic time scale τ of the nonequilibrium noise source (4). It is obtained from numerical simulations of model (1) with the potential of Fig. 1 and periodic driving (4). The dimensionful parameter values are chosen as in Fig. 2. The lines interconnecting the dots serve as a guide to the eye. For even larger τ (not shown), a very small, negative asymptotic value is approached from below (cf. Fig. 5).

nism as detailed above. Consequently, also the resulting ANM is more pronounced, thereby explaining the observed bursting of ANM in Fig. 4.

C. Slow driving

The slow-driving regime is characterized by sojourn times τ of the nonequilibrium source (4), which are much longer than the mean escape time out of a trap for the forces contributing in Eq. (10). In view of $\tau_{esc}(A+F) > \tau_{esc}(A-F)$, see Eq. (19) below, this implies that

$$\tau \gg \tau_{esc}(A+F). \qquad (15)$$

To determine the average traveling distance $\Delta y(\tau, F_{tot})$ for such large τ values, we start by calculating the time to advance by one period L along the y axis for $F_{tot}>0$: With probability p approximately given in Eq. (12), the particle avoids the trap within such a period; its traveling time to cover the period L is then approximately given by

$$\tau_L := \frac{L}{v_y} = \frac{L\eta}{F_{tot}}, \qquad (16)$$

wherein we have exploited Eq. (11) for the second equality. With probability $1-p$, the particle gets trapped and has to reescape from the trap in order to cover the period L; this in turn yields an increase of the traveling time by τ_{esc} on the average. The average time to advance by one period L is therefore $pL/v_y + [1-p][L/v_y + \tau_{esc}(F_{tot})]$. With Eq. (16), the resulting average traveling distance during the (large) time $\tau \gg \tau_{esc}(F_{tot})$ then takes the form

$$\Delta y(\tau, F_{tot}) = \frac{\tau L}{(L\eta/F_{tot}) + [1-p(F_{tot})]\tau_{esc}(F_{tot})}. \qquad (17)$$
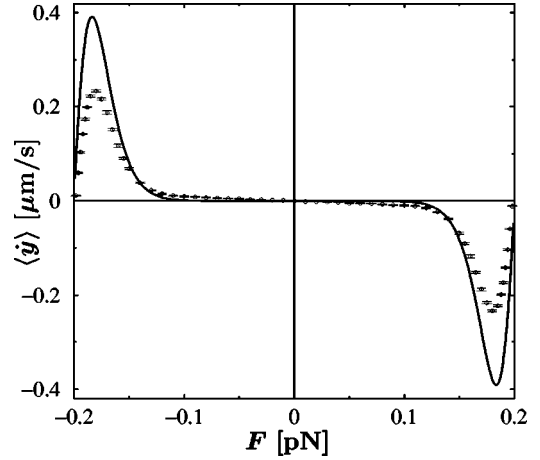

FIG. 5. Current-load characteristics for Eq. (1) with the potential $V(x,y)$ of Fig. 1, periodic driving (4), and the same parameter values as in Fig. 2 except for $\tau=25$ s. Dots with error bars show numerical simulations of Eq. (1). Solid lines: analytic approximation (10) with Eqs. (17) and (19).

For small $F_{tot}>0$, the effect of the traps is small and the first term in the denominator of Eq. (17) dominates. Hence, Δy *increases* in the expected linear response manner with increasing F_{tot}. As F_{tot} becomes larger, $1-p$ approaches 1, cf. Eq. (12), and the escape time τ_{esc} increases very fast, cf. Eq. (19) below. This increasing "stickiness" or "depth" of the traps with increasing F_{tot} [2,4,5,35–38,59,60] implies the existence of a maximum and a subsequent *decay* of Δy. As a consequence we recover once again ANM in Eq. (10) for sufficiently large A, based on the mechanism that the particle travels on average *shorter* distances for *larger* applied forces F_{tot}. This prediction of ANM is confirmed by the numerical simulations shown in Fig. 5. Moreover, the agreement of the simulations with Eq. (10) and Eqs. (17) and (19) below is satisfactory.

To approximate the mean escape time τ_{esc}, the two-dimensional geometrical trap is reduced to a one-dimensional potential system according to the following procedure: Out of the entire corridor we consider only a small part consisting of one corner [i.e., a segment of the (left) corridor wall with an obstacle attached to it], and a particle being trapped in this corner by the external force $F_{tot}>0$. Neglecting the effect of the wall, the motion of the particle decouples into a component parallel to the obstacle and a component perpendicular to it. We thus may consider only the one-dimensional motion along the auxiliary coordinate $X=x/\sin\theta$ parallel to the obstacle, which is governed by thermal fluctuations and by the external force component $F_{tot}\cos\theta$. The corresponding one-dimensional Langevin equation reads

$$\eta\dot{X}(t) = -F_{tot}\cos\theta + \xi_X(t), \qquad (18)$$

where $\xi_X(t)$ represents the thermal Gaussian fluctuations with the properties specified in Eq. (2). This dynamics correctly reproduces the equilibrium distribution as well as the limiting case of zero temperature $T=0$. One can then ap-
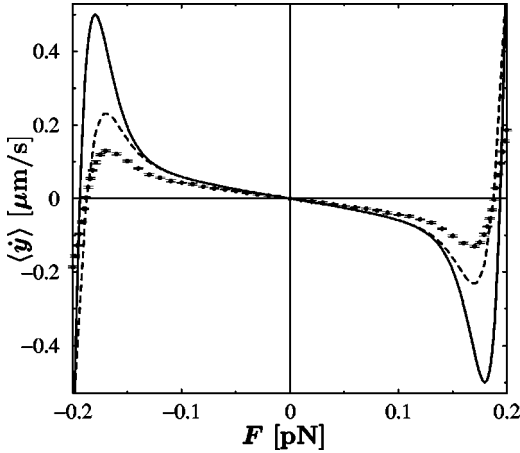
FIG. 6. Current-load characteristics for Eq. (1) with the potential $V(x,y)$ of Fig. 1, periodic driving (4), and the same parameter values as in Fig. 2 except for $\tau = 5$ s. Dots with error bars: numerical simulations of Eq. (1). Solid lines show analytic approximation by adding up Eqs. (13) and (17) and then evaluating Eq. (10). Dashed lines show analytic approximation based on Eqs. (21), (22), and (24) as described in more detail in the main text.

proximate $\tau_{\mathrm{esc}}(F_{\mathrm{tot}})$ by the mean first passage time from $X = 0$ to $X = b/\sin\theta$ with a reflecting boundary placed at $X = 0$ [40] to obtain

$$\tau_{\mathrm{esc}}(F_{\mathrm{tot}}) = \frac{b^2 \eta}{k_B T} \frac{e^\alpha - \alpha - 1}{\alpha^2 \sin^2\theta},$$

$$\alpha := b \, F_{\mathrm{tot}} \cot\theta/k_B T. \tag{19}$$

D. Driving with arbitrary period

The upshot of our present findings in this section is two-fold. On the one hand, we showed that ANM occurs for both, (moderately) fast driving and (asymptotically) slow driving as characterized by (14) and (15). On the other hand, the respective physical origins of ANM, being quantitatively captured by Eqs. (13) and (17), turned out to be *completely different*: In the fast-driving regime, transient, force-dependent "first-trapping events" after each jump of F_{tot} provide the crucial mechanism for ANM, while in the slow-driving regime "reescape events" out of the traps are responsible for ANM. These escape events are negligible for fast driving, while for slow driving the transient behavior is irrelevant. In other words, the pivotal mechanism creating ANM in one case is completely negligible for the other case and vice versa. Thus, our model (1) (with the potential of Fig. 1) reveals the remarkable feature that two completely different, "complementary" physical mechanisms both support one and the same phenomenon. On the basis of this physical insight, we may naively expect that ANM will be present as a result of a "superposition" of both effects in the intermediate driving regime as well. An educated guess is thus to add Eqs. (13) and (17) and then evaluate Eq. (10). These predictions are nicely confirmed by Fig. 6.

For a more sophisticated and systematic analysis of general driving, we start by extending our approach of Sec. III C

by taking into account the distribution $\psi_{\mathrm{esc}}(t)$ of escape times out of the traps. This distribution can be approximated by

$$\psi_{\mathrm{esc}}(t) = \frac{1}{\tau_{\mathrm{esc}}} e^{-t/\tau_{\mathrm{esc}}}. \tag{20}$$

Similar in spirit as for the derivation of the mean time, a particle needs to cover a period L [see above Eq. (17)]; we now obtain a distribution $\psi(t)$ of traveling times (for $F_{\mathrm{tot}} > 0$). When the trap within such a period is avoided, this time is given by τ_L from Eq. (16). In contrast, when the particle's motion is held up by the trap, the traveling time is distributed according to $\psi_{\mathrm{esc}}(t)$ with an additional "time off-set" τ_L that represents the drift across this period. The respective probabilities p and $1 - p$ are approximated by Eq. (12). Therefore, we find

$$\psi(t) = p \, \delta(t - \tau_L) + (1 - p) \, \Theta(t - \tau_L) \psi_{\mathrm{esc}}(t - \tau_L), \tag{21}$$

where $\Theta(t)$ is the Heaviside function and the argument F_{tot} has been omitted in p and τ_{esc}. This result is based on our assumption that the particle always closely passes by the leftmost edge of any obstacle attached to the right corridor wall when $F_{\mathrm{tot}} > 0$, as indicated in Fig. 3(a). Furthermore, we have again neglected the fact that the "free traveling speed" (11) slightly decreases when the particle "slides down on the back" of an obstacle. As an important consequence of these two approximations, the traveling times across any period L are governed by one and the same probability distribution $\psi(t)$ given by Eq. (21), independent of the particle's past history (Markov property), and independent of the concrete partition of the "corridor" along the y direction into segments of period L.

In this way, the original two-dimensional system (1) (with the potential of Fig. 1) is approximately reduced to a one-dimensional, unidirectional random walk characterized by $\psi(t)$, Eq. (21). Provided that the random walk advances in discrete steps ("hopping process"), such problems have been analyzed in detail in the context of renewal theory [61,62]. Extending these methods to our case of continuous motion (see the Appendix), we obtain for the Laplace transformed displacement $\Delta \tilde{y}(s, F_{\mathrm{tot}}) := \int_0^\infty dt \, \Delta y(t, F_{\mathrm{tot}}) e^{-ts}$ the result [63]

$$\Delta \tilde{y}(s, F_{\mathrm{tot}}) = \frac{L}{s} \frac{\tilde{\psi}(s)}{1 - \tilde{\psi}(s)} \frac{e^{\tau_L s} - 1}{\tau_L s}, \tag{22}$$

where

$$\tilde{\psi}(s) = e^{-s\tau_L} \frac{1 + p s \tau_{\mathrm{esc}}}{1 + s \tau_{\mathrm{esc}}} \tag{23}$$

is the Laplace transform of $\psi(t)$ from Eqs. (20) and (21). The expression (22) differs from standard renewal theory [61,62] by the last factor on the right hand side, which accounts for the fact that the particle proceeds continuously rather than in discrete jumps of length L. After an inverse Laplace transformation of Eq. (22), a final transformation,

$$\Delta y(\tau,F_{tot}) \mapsto \begin{cases} v_y\tau & \text{if } \tau < 3L/2v_y, \\ \Delta y(\tau - 3L/2v_y, F_{tot}) + 3L/2 & \text{if } \tau \geq 3L/2v_y, \end{cases}$$
(24)

is required, because the "basic distance" of approximately $3L/2$, which the particle covers before encountering the first trap [see Fig. 3 and below Eq. (12) below], is not yet taken into account by Eq. (22). The distinction between the two cases in Eq. (24) can be understood as follows: On its way to the first trap, the particle proceeds with approximately the free traveling speed v_y from Eq. (11). It thus can cover the "basic distance" $3L/2$ only if τ is sufficiently large, namely, $\tau \geq 3L/2v_y$; for smaller τ, the particle advances by the distance $v_y\tau$. With the average traveling distances finally obtained from Eq. (24), current (5) follows according to Eq. (10). A typical result is depicted in Fig. 6, being in good agreement with the numerical simulations. Moreover, it presents a notable improvement in comparison to the naive first guess discussed above.

While a numerical evaluation of the inverse Laplace transformation is necessary in general, the special cases of moderately fast and slow driving detailed in Secs. III A and III C can be treated analytically. The basic assumption for fast driving that a trapped particle does not escape from its trap corresponds to the limit $\tau_{esc} \to \infty$ in Eq. (20); the probability for escaping from the trap within any finite time t is then zero. In this limit, Eq. (23) simplifies to $p\,e^{-s\tau_L}$. Then, the transformation to original time in Eq. (22) is straightforward, and, by additionally taking into account the final transformation (24), one recovers the previous (moderately) fast driving result (13), provided that $\tau/\tau_L - 3/2 \in \mathbb{N}$ (for details, see the Appendix). Slow driving is characterized by (very) large sojourn times with constant total force (9), see Eq. (15). We expect that such an asymptotic long-time limit of Δy is related to the small-s behavior of $\Delta\tilde{y}$, for which we find

$$\Delta\tilde{y}(s,F_{tot}) = \frac{1}{s^2}\frac{L}{\tau_L + (1-p)\tau_{esc}} \quad \text{as } s \to 0. \quad (25)$$

This guess is mathematically rigorously corroborated by a so-called Tauberian theorem [61,64]: If for constants J and K,

$$\tilde{h}(s) = \frac{J}{s^2} + \frac{K}{s} + O(1) \quad \text{as } s \to 0 \quad (26)$$

for the Laplace transform $\tilde{h}(s)$ of a function $h(\tau)$, then

$$h(\tau) = J\tau + K + o(1) \quad \text{as } \tau \to \infty. \quad (27)$$

In Eq. (26), $O(1)$ denotes a function of s which is bounded as $s \to 0$, whereas $o(1)$ in Eq. (27) denotes a function of τ tending to zero as $\tau \to \infty$. In view of this theorem and expansion (25), we herewith recover our previous result (17).

IV. GENERALIZATIONS

The model (1), (4) together with the potential landscape of Fig. 1 is particularly suitable for elucidating the different basic physical mechanisms for ANM, and for quantifying them by simple theoretical concepts. Based on the so-gained physical insight, we expect that ANM subsists for various generalizations and modifications of our original model, thereby providing a whole collection of systems containing noninteracting classical Brownian particles that are capable of exhibiting ANM. In the following, we discuss several such generalizations, mainly with respect to the form of the potential landscape and/or the nonequilibrium perturbation. Restricting ourselves to a more qualitative level in these discussions, we shall present corresponding simulation results of Eq. (1) in dimensionless units.

A. Dichotomous noise

As already alluded to in Sec. II, the simplest nonequilibrium model $\zeta_y(t)$ in Eq. (1) is, from a theoretical viewpoint, a symmetric dichotomous noise that switches randomly between two states $\pm A$ with a switching rate γ. This case of a nonequilibrium perturbation can be understood along the same qualitative arguments as already developed for periodic driving (4) in the preceding section. We therefore conclude that ANM occurs due to the same physical mechanisms at work [28]. However, the current (5) now results from the contribution of all sojourn times τ of the total forcing states $F_{tot} = F \pm A$ according to the distribution $\rho(\tau)$ from Eq. (3). Consequently, the current formula (10) generalizes to

$$\langle \dot{y} \rangle = \frac{\displaystyle\int_0^\infty d\tau\,\rho(\tau)[\Delta y(\tau, A+F) - \Delta y(\tau, A-F)]}{2\displaystyle\int_0^\infty d\tau\,\rho(\tau)\tau}, \quad (28)$$

wherein the average traveling distance $\Delta y(\tau, F_{tot})$ has, in general, to be calculated from Eqs. (22) and (24). To determine the mean escape time τ_{esc} required in Eq. (22), one must take into account that the dichotomous perturbation $\zeta_y(t)$ does not contain a thermal noise part. The thermal bath thus only couples to the x component of model (1). As a consequence, the relevant effective temperature of the thermal noise $\xi_X(t)$ in Eq. (18) is given by $T_{eff} = T\sin^2\theta$, resulting in a similar replacement $T \mapsto T\sin^2\theta$ in Eq. (19).

Instead of the generally valid formula (22) for the traveling distance Δy, we may, in some special cases of the distribution $\rho(\tau)$, employ in Eq. (28) the high- or low-frequency results (13) or (17), respectively. If, e.g., large sojourns τ dominate, then the average traveling distance Δy may be approximated by Eq. (17). As a consequence, $\Delta y(\tau, F_{tot})/\tau$ becomes independent of τ, and thus Eq. (28) resimplifies to Eq. (10). On the other hand, for large enough rates γ in Eq. (3) (small sojourn times τ predominate), the average traveling distances $\Delta y(\tau, F_{tot})$ [which noticeably contribute in Eq. (28)], may be well captured by the fast-driving result (13). A typical example of such a theoretical estimate is depicted with Fig. 7, in good agreement with the numerical simulations.

It is quite clear that the above discussion and especially Eq. (28) with Eqs. (22) and (24) is not restricted to dichotomous noise $\zeta_y(t)$, but can be taken over without any change for arbitrary random as well as deterministic processes $\zeta_y(t)$
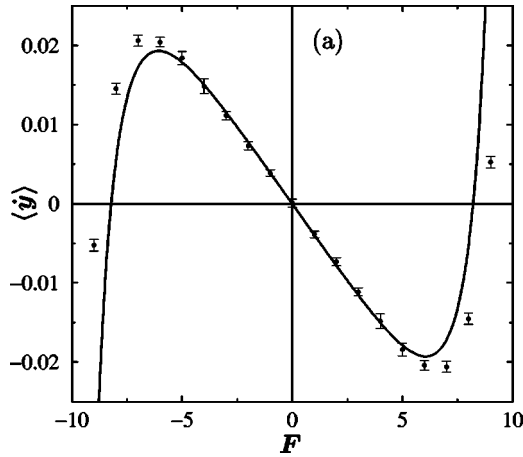
FIG. 7. Current-load characteristics for Eq. (1) with the potential $V(x,y)$ of Fig. 1, dichotomous noise (3), and dimensionless parameter values $L=1$, $B=1$, $b=0.55$, $\theta=45°$, $k_BT=0.1$, $\eta=1$, $A=10$, $\gamma=0.4$. Dots with error bars show numerical simulations of Eq. (1). The solid line shows analytic approximation (28) with Eqs. (12) and (13).

switching between $\pm A$ according to some switching time distribution $\rho(\tau)$. Returning finally to the special case of a dichotomous process $\zeta_y(t)$ with Eq. (3) one sees that the numerator in Eq. (28) can be evaluated in terms of the Laplace transform $\Delta\widetilde{y}(s,F_{\text{tot}})$. Taking into account the transformation (24), one then obtains the explicit analytical result

$$\langle\dot{y}\rangle = \frac{F}{\eta} - \frac{L}{2}\left[\frac{e^{-(3/2)\gamma\tau_L^+}}{\tau_L^+}\frac{1-\widetilde{\psi}^+(\gamma)e^{\gamma\tau_L^+}}{1-\widetilde{\psi}^+(\gamma)}\right.$$
$$\left. - \frac{e^{-(3/2)\gamma\tau_L^-}}{\tau_L^-}\frac{1-\widetilde{\psi}^-(\gamma)e^{\gamma\tau_L^-}}{1-\widetilde{\psi}^-(\gamma)}\right], \qquad (29)$$

where the superscripts $\pm$ refer to the total forces $A\pm F$. In Eq. (29), $\tau_L^\pm$ follows from Eq. (16) and $\widetilde{\psi}^\pm(\gamma)$ from Eq. (23); the required probability p is obtained according to Eq. (12) and the modified mean escape time τ_{esc} according to Eq. (19), with $T\mapsto T\sin^2\theta$.

B. Alternative potential landscapes

The most immediate geometrical modification of the potential from Fig. 1 is shown in Fig. 8, where the corridor of Fig. 1 is periodically continued along the x direction. Due to obvious symmetry properties of the dynamics (1), the current (5) through this sieve remains exactly the same as in Fig. 1, but the parallelization now admits to simultaneously transport many more particles. This "sieve" is reminiscent of the two-dimensional arrays of obstacles theoretically considered in Refs. [65–67]. We emphasize, however, that the physical phenomena studied there are completely different from ours; in particular ANM has not been addressed in those works.

Yet alternative corridors are depicted in Fig. 9. They all do not possess obstacles, but provide traps with increasing stickiness as the bias forces (along the y axis) increase. Consequently, ANM is found in the slow-driving regime accord-
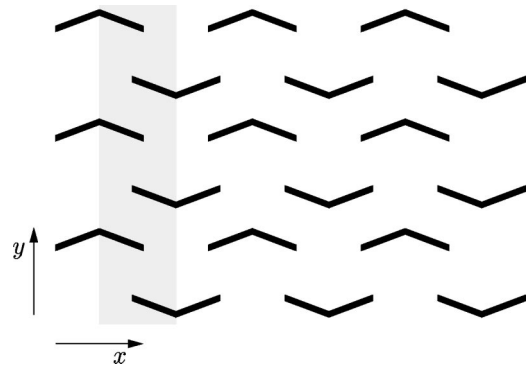

FIG. 8. Hard-wall potential $V(x,y)$ like in Fig. 1 but now periodically continued along the x axis, resulting in a two-dimensional array of obstacles ("sieve"). For symmetry reasons, the y component of the Brownian motion (1) is completely independent of whether the gray shaded "corridor" is endowed with perfectly reflecting "sidewalls" (Fig. 1) or not.

ing to the very same mechanism as discussed in Sec. III C. Under (moderately) fast nonequilibrium perturbations, however, the potential landscapes from Fig. 9 behave quite different from those of Figs. 1 and 8. In the corridor of Fig. 9(a), the particle gets trapped by "falling into a depression" when "sliding down the ramps." Due to the additional diffusive motion, this trapping occurs with higher probability
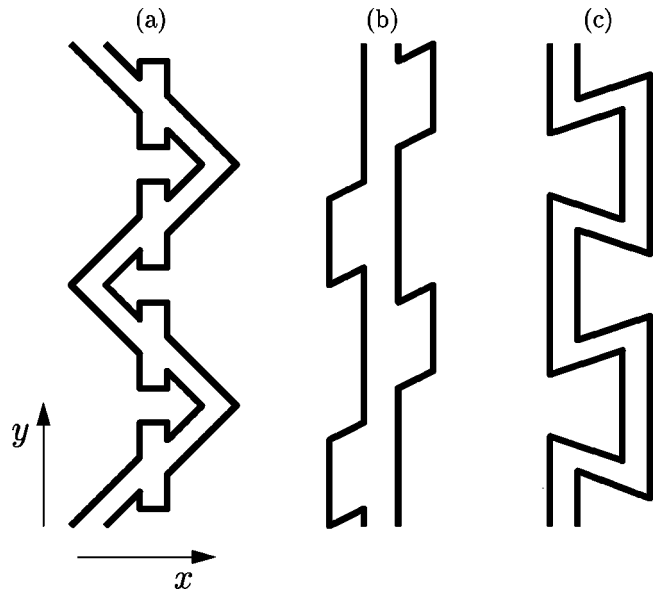

FIG. 9. Alternative geometries for hard-wall corridors with traps that may represent the potential $V(x,y)$ in Eq. (1) to yield ANM. In each case, the particle is confined to the inner white regions where $V(x,y)\equiv0$; the black walls are defined to have infinite potential. All these corridors are periodic (shown are two periods) and symmetric with respect to inversion of the y axis. (a) The vertical parts of the corridor act as traps. The particle "falls into" them when "sliding down the diagonal ramps." (b) The traps are represented by the attached "fins" and are entered by lateral diffusion along the x direction while "falling" along the central "backbone." (c) The particle is trapped in the "corners" with a probability that is practically 1, independent of the strength of the force F_{tot}.

the faster the "free fall" with velocity v_y from Eq. (11) proceeds, and thus the larger the total external force (9) is. As discussed in Sec. III A, such a force-dependent trapping probability of the particle implies ANM for (moderately) fast driving. The potential landscape of Fig. 9(b), does not support this mechanism. Here, faster drift along the y direction even *decreases* the trapping probability. Similarly, fast-driving ANM based on force-dependent trapping processes cannot occur with Fig. 9(c), since the trapping probability (in the corners) is practically 1, independent of the external force strength.

V. CONCLUSIONS

In this paper, we have demonstrated that a single, classical Brownian particle in a periodic, symmetric, two-dimensional potential landscape can exhibit the paradoxical and *prima facie* quite astonishing phenomenon of absolute negative mobility under suitable far from equilibrium conditions. This constitutes a substantial simplification and extension in comparison to the physical systems hitherto known to exhibit ANM, where either quantum mechanical effects [2–12] or else particle-particle interactions [23–27] are clearly indispensable for the emergence of ANM.

The qualitative and quantitative analysis of the ANM phenomenon in such classical, one-particle systems has been exemplified in detail for periodic nonequilibrium perturbations (4) in Eq. (1) and the potential landscape from Fig. 1. The main analytical result is the Laplace-transformed average traveling distance Eq. (22) from which the particle current is obtained (after an inverse Laplace transformation) according to (10). The occurrence of ANM is found to be robust against various modifications of the potential landscape and the nonequilibrium noise source. In general, it is simultaneously supported by completely different physical mechanisms that dominate in the distinct driving regimes (fast vs slow) of the nonequilibrium perturbations [28]. These different mechanisms have in common that they all exploit the existence of "particle traps," which is, in fact, the characteristic feature of the potential landscapes considered herein. Put differently, *any* potential landscape that provides traps with increasing stickiness as the external force strengths increase is expected to exhibit ANM, at least for adiabatically slow nonequilibrium perturbations [2,4,5]. A well-known system of this kind is the two-dimensional gel network consisting of randomly distributed traps which is used in trapping electrophoresis for DNA-protein complexes [59,60].

Experimental implementations of the ANM effect can be realized with mechanical microsystems of the type discussed herein. Likewise, other potential realizations involve the Brownian motion of colloidal particles in light-guided tracks or the motion of atoms and molecules in appropriately designed optical lattices [68]. Extensions of our basic ideas to Coulomb blockade systems [69,70] represent promising applications.

Apart from the phenomenon of absolute negative mobility itself, other future challenges involve the problem of optimization of ANM as a function of the parameters that characterize the nonequilibrium situation. Moreover, a single realization exhibits mobility fluctuations that depend on the diffusive properties of the driven Brownian motion process. The diffusion of the displacements present yet another objective that is worthwhile to be addressed in the future in greater detail.

APPENDIX: CONTINUOUS UNI-DIRECTIONAL RANDOM WALK

Interpreting the motion of the particle for the moment within a coarse grained approximation of $y(t)$ by multiples of L as a hopping process characterized by some waiting time distribution $\psi(t)$, we can readily derive the Laplace transform $\Delta \tilde{y}(s,F_{\text{tot}})$ of the average traveling distance $\Delta y(t,F_{\text{tot}})$ according to the usual renewal theory [61,62]: The probability $P(n,t)$ to make n steps within the time t is given by the sum over the probabilities of all possible realizations of the random walk, namely, a first step at time t_1 $(0<t_1<t)$, a second step at time t_1+t_2 $(t_1+t_2<t$ and $t_2>0)$, etc., and the $(n+1)^{\text{th}}$ step at time $t_1+\cdots+t_{n+1}$ *later* than t [62],

$$P(n,t)=\int_0^t dt_1\,\psi(t_1)\int_0^{t-t_1}dt_2\psi(t_2)\cdots\int_0^{t-t_1-\cdots-t_{n-1}}dt_n\psi(t_n)\int_{t-t_1-\cdots-t_n}^{\infty}dt_{n+1}\psi(t_{n+1}). \tag{A1}$$

Once $P(n,t)$ is known, $\Delta y(t,F_{\text{tot}})$ readily follows according to

$$\Delta y(t,F_{\text{tot}})=L\sum_{n=0}^{\infty}n\,P(n,t). \tag{A2}$$

After a Laplace transformation, one obtains the well-known result [61,62]

$$\Delta \tilde{y}(s,F_{\text{tot}})=\frac{L}{s}\frac{\tilde{\psi}(s)}{1-\tilde{\psi}(s)}, \tag{A3}$$

where $\widetilde{\psi}(s)$ is the Laplace transform of $\psi(t)$.

However, this discrete approximation clearly does not capture the continuous motion of the particle properly. Nevertheless, we can describe all periods L that the particle passes *completely* during the time t by such a hopping process, since the dynamical details within these periods are of no interest [they are fully incorporated in the waiting time distribution $\psi(t)$]. Only within the "final period" (which will not be passed completely) the continuous motion of the particle has to be taken into account explicitly. To this end, we approximate that continuous motion by a hopping process with step size $\delta L := L/K$, where $K \in \mathbb{N}$ (K large) is the number of steps to cover the period L completely. The coordinate y is thus discretized according to

$$y = nL + k\,\delta L, \qquad (A4)$$

where $n \in \mathbb{N}_0$ is the number of complete periods contained in y and $k = 0,1, \ldots, K-1$ represents the position within the period $n+1$. Finally, after $\Delta \widetilde{y}(s, F_{\mathrm{tot}})$ for this coarse grained approximation has been calculated, we perform the limit $K \to \infty$ (implying $\delta L \to 0$) to regain a genuine continuous motion.

Due to this approach, we can still apply renewal theoretic methods. The particle motion is now characterized by the following three waiting time distributions [cf. Eq. (21)]

$$\psi(t) = p\,\delta(t - \tau_{\mathrm{L}}) + (1-p)\Theta(t - \tau_{\mathrm{L}})\psi_{\mathrm{esc}}(t - \tau_{\mathrm{L}}), \qquad (A5a)$$

$$\psi_{\delta L}(t) = \delta(t - \tau_{\mathrm{L}}/K), \qquad (A5b)$$

$$\psi_{\mathrm{trap},\delta L}(t) = p\,\delta(t - \tau_{\mathrm{L}}/K)$$
$$+ (1-p)\Theta(t - \tau_{\mathrm{L}}/K)\psi_{\mathrm{esc}}(t - \tau_{\mathrm{L}}/K), \qquad (A5c)$$

where $\psi_{\mathrm{esc}}(t)$ is the distribution of escape times out of a trap. As in Eq. (21), Eq. (A5a) represents the traveling times through any (full) period L. The distributions (A5b) and (A5c) describe the motion within a period, where Eq. (A5c) accounts for the single step that passes by the trap contained in this period. Note that both these distributions (A5b) and (A5c) depend on the step size δL, since $\tau_{\mathrm{L}}/K = \delta L/v_y$. The Laplace transforms of the distributions (A5) read

$$\widetilde{\psi}(s) = e^{-s\tau_{\mathrm{L}}}[p + (1-p)\widetilde{\psi}_{\mathrm{esc}}(s)], \qquad (A6a)$$

$$\widetilde{\psi}_{\delta L}(s) = e^{-s\tau_{\mathrm{L}}/K}, \qquad (A6b)$$

$$\widetilde{\psi}_{\mathrm{trap},\delta L}(s) = e^{s\tau_{\mathrm{L}}(1-1/K)}\widetilde{\psi}(s), \qquad (A6c)$$

with $\widetilde{\psi}_{\mathrm{esc}}(s)$ denoting the Laplace transform of $\psi_{\mathrm{esc}}(t)$.

In order to calculate the average traveling distance $\Delta y(t, F_{\mathrm{tot}})$ via its Laplace-transformed counterpart $\Delta \widetilde{y}(s, F_{\mathrm{tot}})$, we now consider the probability $P(n,k,t)$ to cover n periods L completely and to additionally make k steps in the "final period" $n+1$ during the total time t. Similarly as in Eq. (A1), it is given by

$$P(n,k,t) = \int_0^t dt_1 \psi(t_1) \int_0^{t-t_1} dt_2 \psi(t_2) \cdots \int_0^{t-t_1-\cdots-t_{n-1}} dt_n \psi(t_n) P(0,k,t-t_1-\cdots-t_n). \qquad (A7)$$

In comparison to Eq. (A1), the last integral has been replaced by the probability $P(0,k,t-t_1-\cdots-t_n)$ to advance by k steps of size δL during the remaining time $t-t_1-\ldots-t_n$. This probability is given by

$$P(0,k,t) = \begin{cases} \displaystyle\int_t^\infty dt_1 \psi_{\mathrm{trap},\delta L}(t_1) & \text{for } k=0, \\[1em] \displaystyle\int_0^t dt_1 \psi_{\mathrm{trap},\delta L}(t_1) \int_0^{t-t_1} dt_2 \psi_{\delta L}(t_2) \cdots \int_0^{t-t_1-\cdots-t_{k-1}} dt_k\, \psi_{\delta L}(t_k) \int_{t-t_1-\cdots-t_k}^\infty dt_{k+1}\psi_{\delta L}(t_{k+1}) & \text{for } k>0. \end{cases} \qquad (A8)$$

Here, we have exploited the possibility to freely choose the partition of the corridor into periods of length L, as discussed in Sec. III D. We take a period to start just before a trap and to end just before the next trap which is consistent with the initial "basic distance" captured by the final transformation (24), see also Fig. 3. Consequently, we have to take into account the trap in the *first* small step ($k=1$) by using the distribution (A5c). Then, the right-hand sides of Eq. (A8) follow according to the same line of reasoning that has led us to Eq. (A1).

The traveling distance $\Delta y(t, F_{\mathrm{tot}})$ is obtained by averaging [cf. (A2)],

$$\Delta y(t, F_{\mathrm{tot}}) = \sum_{n=0}^{\infty} \sum_{k=0}^{K-1} (nL + k\,\delta L) P(n,k,t). \qquad (A9)$$

Using the Laplace transform of the probability $P(n,k,t)$,

$$\widetilde{P}(n,k,s) = \begin{cases} \dfrac{1}{s}[\widetilde{\psi}(s)]^n[1-\widetilde{\psi}_{\text{trap},\delta L}(s)] & \text{for } k=0 \\[3mm] \dfrac{1}{s}[\widetilde{\psi}(s)]^n\widetilde{\psi}_{\text{trap},\delta L}(s)[\widetilde{\psi}_{\delta L}(s)]^{k-1}[1-\widetilde{\psi}_{\delta L}(s)] & \text{for } k>0, \end{cases} \tag{A10}$$

and taking into account Eqs. (A6b) and (A6c), a somewhat tedious but straightforward calculation yields for the Laplace-transformed average traveling distance [cf. Eq. (A3)],

$$\Delta\widetilde{y}(s,F_{\text{tot}}) = \frac{L}{s}\frac{\widetilde{\psi}(s)}{1-\widetilde{\psi}(s)}\frac{e^{s\tau_{\text{L}}}-1}{K(e^{s\tau_{\text{L}}/K}-1)}. \tag{A11}$$

Taking the continuous-space limit $K\to\infty$, we obtain [63] our final result [cf. Eq. (22)]

$$\Delta\widetilde{y}(s,F_{\text{tot}}) = \frac{L}{s}\frac{\widetilde{\psi}(s)}{1-\widetilde{\psi}(s)}\frac{e^{\tau_{\text{L}}s}-1}{\tau_{\text{L}}s}. \tag{A12}$$

As already mentioned in Sec. III D, the inverse Laplace transformation of Eq. (A12) has to be performed, in general, numerically. However, for the specific form (20) of the escape time distribution $\psi_{\text{esc}}(t)$, an analytical backtransformation is feasible in the limit $\tau_{\text{esc}}\to\infty$, which corresponds to the fast-driving regime discussed in Sec. III A. For this limit, the Laplace transform (23) of the waiting time distribution $\psi(t)$ simplifies to

$$\widetilde{\psi}(s) = pe^{-s\tau_{\text{L}}}. \tag{A13}$$

Observing that $\widetilde{\psi}(s)/[1-\widetilde{\psi}(s)] = \sum_{n=1}^{\infty}[\widetilde{\psi}(s)]^n$, the Laplace-transformed average traveling distance (A12) for this case reads

$$\Delta\widetilde{y}(s,F_{\text{tot}}) = \frac{L}{s}\frac{e^{\tau_{\text{L}}s}-1}{\tau_{\text{L}}s}\sum_{n=1}^{\infty}p^n e^{-ns\tau_{\text{L}}}. \tag{A14}$$

The inverse Laplace transform is

$$\Delta y(t,F_{\text{tot}}) = \frac{L}{2\pi i}\sum_{n=1}^{\infty}\frac{p^n}{\tau_{\text{L}}}\int_{-i\infty+\lambda}^{+i\infty+\lambda}ds\frac{1}{s^2}e^{-ns\tau_{\text{L}}}(e^{s\tau_{\text{L}}}-1)$$

$$= L\sum_{n=1}^{\infty}\frac{p^n}{\tau_{\text{L}}}\{[t-(n-1)\tau_{\text{L}}]\Theta[t-(n-1)\tau_{\text{L}}]$$

$$-(t-n\tau_{\text{L}})\Theta(t-n\tau_{\text{L}})\} \tag{A15}$$

by the theorem of residues, where λ must be chosen such that all poles of the integrand in the complex plane of s are located to the left of the integration path. With the definition $\mathcal{N} := [t/\tau_{\text{L}}]_{\text{int}}$ (where $[\,\cdot\,]_{\text{int}}$ denotes the largest integer smaller than the enclosed expression), the first sum terminates at $\mathcal{N}+1$, the second at $\mathcal{N}$, and we obtain

$$\Delta y(t,F_{\text{tot}}) = -1 + \frac{1-p^{\mathcal{N}+1}}{1-p} + p^{\mathcal{N}+1}(t/\tau_{\text{L}}-\mathcal{N}). \tag{A16}$$

Finally, inserting $\mathcal{N} = [t/\tau_{\text{L}}]_{\text{int}} = [F_{\text{tot}}t/\eta L]_{\text{int}}$ [cf. Eq. (16)] and taking into account the transformation (24) (for $t>3L/2v_y$), we end up with the result

$$\Delta y(t,F_{\text{tot}}) = L\left\{\frac{1}{2} + \frac{1-[p(F_{\text{tot}})]^{[F_{\text{tot}}t/(\eta L)-1/2]_{\text{int}}}}{1-p(F_{\text{tot}})}\right.$$

$$+ [p(F_{\text{tot}})]^{[F_{\text{tot}}t/(\eta L)-1/2]_{\text{int}}}$$

$$\left.\times\left(\frac{F_{\text{tot}}t}{\eta L}-\frac{3}{2}\right)\bmod 1\right\}, \tag{A17}$$

where mod is the usual modulo operator. The first two terms represent the average number of periods, L, that the particle can cover completely within the time t including the "basic distance" $3L/2$ [see also Eq. (13)]. The last term accounts for the situation where the particle passes through $N=[t/\tau_{\text{L}}-3/2]_{\text{int}}$ periods without being trapped, afterwards it also avoids the next trap (with absolute probability p^{N+1}) and proceeds further for the remaining time $t-(3/2+N)L/v_y$. This latter possibility has been neglected in the derivation of our moderately fast-driving result (13) in Sec. III A. Consequently, Eqs. (13) and (A17) are identical only if $t/\tau_{\text{L}}-3/2 \in \mathbb{N}$. Otherwise, Eqs. (13) and (A17) constitute two different possibilities for a "smooth interpolation," where obviously Eq. (A17) is the physically correct one. However, for all the cases considered in this paper (Figs. 2, 6, and 7), the differences between Eqs. (13) and (A17) are extremely small.

---

[1] B. Cleuren and C. Van den Broeck, Europhys. Lett. **54**, 1 (2001).

[2] T.Y. Banis, I.V. Parshelyunas, and Y.K. Pozhela, Fiz. Tekh. Poluprovodn. **5**, 1990 (1971) [Sov. Phys. Semicond. **5**, 1727 (1972)].

[3] V.V. Pavlovich and E.M. Épshteĭn, Fiz. Tekh. Poluprovodn. **10**, 2001 (1976) [Sov. Phys. Semicond. **10**, 1196 (1976)].

[4] J. Pozhela, *Plasma and Current Instabilities in Semiconductors* (Pergamon Press, Oxford, 1981).

[5] T.C.L.G. Sollner, E.R. Brown, W.D. Goodhue, and H.Q. Le, in

Physics of Quantum Electron Devices, edited by F. Capasso, Springer Series in Electronics and Photonics Vol. 28 (Springer, Berlin, 1990), pp. 147–180.

[6] B.J. Keay, S. Zeuner, S.J. Allen, K.D. Maranowski, A.C. Gossard, U. Bhattacharya, and M.J.W. Rodwell, Phys. Rev. Lett. **75**, 4102 (1995).

[7] A.A. Ignatov, E. Schomburg, J. Grenzer, K.F. Renk, and E.P. Dodin, Z. Phys. B: Condens. Matter **98**, 187 (1995).

[8] Y. Dakhnovskii and H. Metiu, Phys. Rev. B **51**, 4193 (1995).

[9] R. Aguado and G. Platero, Phys. Rev. B **55**, 12 860 (1997).

[10] L. Hartmann, M. Grifoni, and P. Hänggi, Europhys. Lett. **38**, 497 (1997).

[11] I.A. Goychuk, E.G. Petrov, and V. May, Phys. Lett. A **238**, 59 (1998).

[12] E.H. Cannon, F.V. Kusmartsev, K.N. Alekseev, and D.K. Campbell, Phys. Rev. Lett. **85**, 1302 (2000).

[13] H. Krömer, Phys. Rev. **109**, 1856 (1958).

[14] D.C. Mattis and M.J. Stevenson, Phys. Rev. Lett. **3**, 18 (1959).

[15] P.F. Liao, A.M. Glass, and L.M. Humphrey, Phys. Rev. B **22**, 2276 (1980).

[16] B.I. Sturman and V.M. Fridkin, *The Photovoltaic and Photorefractive Effects in Noncentrosymmetric Materials* (Gordon and Breach, Philadelphia, 1992).

[17] A.G. Aronov and B.Z. Spivak, Zh Éksp. Teor. Fiz., **22**, 218 (1975) [JETP Lett. **22**, 101 (1975)].

[18] M.E. Gershenzon and M.I. Faleǐ, Pis'ma Zh. Éksp. Teor. Fiz. **44**, 529 (1986) [JETP Lett. **44**, 682 (1986)].

[19] M.E. Gershenzon and M.I. Faleǐ, Zh. Éksp. Teor. Fiz. **94**, 303 (1988) [Sov. Phys. JETP **67**, 389 (1988)].

[20] N.A. Dyatko, I.V. Kochetov, and A.P. Napartovich, Pis'ma Zh. Tekh. Fiz. **13**, 1457 (1987) [Sov. Tech. Phys. Lett. **13**, 610 (1987)].

[21] Z. Rozenberg, M. Lando, and M. Rokni, J. Phys. D **21**, 1593 (1988).

[22] P.M. Golovinskiǐ and A.I. Shchedrin, Zh. Tekh. Fiz. **59**, 51 (1989) [Sov. Phys. Tech. Phys. **34**, 159 (1989)].

[23] P. Reimann, R. Kawai, C. Van den Broeck, and P. Hänggi, Europhys. Lett. **45**, 545 (1999).

[24] P. Reimann, C. Van den Broeck, and R. Kawai, Phys. Rev. E **60**, 6402 (1999).

[25] J. Buceta, J.M. Parrondo, C. Van den Broeck, and F.J. de la Rubia, Phys. Rev. E **61**, 6287 (2000).

[26] C. Van den Broeck, I. Bena, P. Reimann, and J. Lehmann, Ann. Phys. (Leipzig) **9**, 713 (2000).

[27] S.E. Mangioni, R.R. Deza, and H.S. Wio, Phys. Rev. E **63**, 041115 (2001).

[28] R. Eichhorn, P. Reimann, and P. Hänggi, Phys. Rev. Lett. **88**, 190601 (2002).

[29] B. Cleuren and C. Van den Broeck, Phys. Rev. E **65**, 030101(R) (2002).

[30] P. Hänggi and R. Bartussek, in *Nonlinear Physics of Complex Systems*, edited by J. Parisi, S. C. Müller, and W. Zimmermann Lecture Notes in Physics Vol. 476 (Springer, Berlin, 1996), pp. 294–308.

[31] F. Jülicher, A. Ajdari, and J. Prost, Rev. Mod. Phys. **69**, 1269 (1997).

[32] R.D. Astumian, Science **276**, 917 (1997).

[33] P. Reimann, Phys. Rep. **361**, 57 (2002).

[34] P. Reimann and P. Hänggi, Appl. Phys. A: Mater. Sci. Process. **75**, 169 (2002).

[35] S.R. White and M. Barma, J. Phys. A **17**, 2995 (1984).

[36] V. Balakrishnan and C. Van den Broeck, Physica A **217**, 1 (1995).

[37] G.A. Cecchi and M.O. Magnasco, Phys. Rev. Lett. **76**, 1968 (1996).

[38] G.W. Slater, H.L. Guo, and G.I. Nixon, Phys. Rev. Lett. **78**, 1170 (1997).

[39] R.K.P. Zia, E.L. Praestgaard, and O.G. Mouritsen, Am. J. Phys. **70**, 384 (2002).

[40] P. Hänggi, P. Talkner, and M. Borkovec, Rev. Mod. Phys. **62**, 251 (1990).

[41] W.D. Volkmuth and R.H. Austin, Nature (London) **358**, 600 (1992).

[42] J. Rousselet, L. Salome, A. Ajdari, and J. Prost, Nature (London) **370**, 446 (1994).

[43] L.P. Faucheux, L.S. Bourdieu, P.D. Kaplan, and A.J. Libchaber, Phys. Rev. Lett. **74**, 1504 (1995).

[44] L.P. Faucheux and A. Libchaber, J. Chem. Soc., Faraday Trans. **91**, 3163 (1995).

[45] L. Gorre-Talini, S. Jeanjean, and P. Silberzan, Phys. Rev. E **56**, 2025 (1997).

[46] L. Gorre-Talini, J.P. Spatz, and P. Silberzan, Chaos **8**, 650 (1998).

[47] Q.-H. Wei, C. Bechinger, D. Rudhardt, and P. Leiderer, Phys. Rev. Lett. **81**, 2606 (1998).

[48] A. van Oudenaarden and S.G. Boxer, Science **285**, 1046 (1999).

[49] J.S. Bader, R.W. Hammond, S.A. Henck, M.W. Deem, G.A. McDermott, J.M. Bustillo, J.W. Simpson, G.T. Mulhern, and J.M. Rothberg, Proc. Natl. Acad. Sci. U.S.A. **96**, 13165 (1999).

[50] R. Bubeck, C. Bechinger, S. Neser, and P. Leiderer, Phys. Rev. Lett. **82**, 3364 (1999).

[51] C.-F. Chou, O. Bakajin, S.W.P. Turner, T.A.J. Duke, S.S. Chan, E.C. Cox, H.G. Craighead, and R.H. Austin, Proc. Natl. Acad. Sci. U.S.A. **96**, 13762 (1999).

[52] C. Bechinger, Q.H. Wei, and P. Leiderer, J. Phys.: Condens. Mater **12**, A425 (2000).

[53] C. Bechinger and E. Frey, J. Phys.: Condens. Matter **13**, R321 (2001).

[54] C. Bechinger, M. Brunner, and P. Leiderer, Phys. Rev. Lett. **86**, 930 (2001).

[55] C. Marquet, A. Buguin, L. Talini, and P. Silberzan, Phys. Rev. Lett. **88**, 168301 (2002).

[56] L.P. Faucheux, G. Stolovitzky, and A. Libchaber, Phys. Rev. E **51**, 5239 (1995).

[57] L.I. McCann, M. Dykman, and B. Golding, Nature (London) **402**, 785 (1999).

[58] P. Hänggi and H. Thomas, Phys. Rep. **88**, 207 (1982).

[59] G.A. Griess and P. Serwer, Biopolymers **29**, 1863 (1990).

[60] C. Desruisseaux, G.W. Slater, and T.B.L. Kist, Biophys. J. **75**, 1228 (1998).

[61] D.R. Cox, *Renewal Theory* (Methuen and Company, London, 1962).

[62] C. Van den Broeck, in *Noise and Nonlinear Phenomena in Nuclear Systems*, edited by J.L. Muñoz-Cobo and F.C. Difilippo (Plenum, New York, 1989).

[63] We remark that the result in Eq. (22) [or Eq. (A12)] is valid for general escape time distributions $\psi_{\mathrm{esc}}(t)$ in Eq. (21), although

we will focus on the special case (20) in the following.

[64] W. Feller, *An Introduction to Probability Theory and Its Applications* (Wiley, New York, 1966), Vol. 2.
[65] D. Ertaş, Phys. Rev. Lett. **80**, 1548 (1998).
[66] T.A.J. Duke and R.H. Austin, Phys. Rev. Lett. **80**, 1552 (1998).
[67] I. Derényi and R.D. Astumian, Phys. Rev. E **58**, 7781 (1998).
[68] G. Grynberg, P. Horak, and C. Mennerat-Robilliard, Europhys. Lett. **49**, 424 (2000).
[69] T. Mii and K. Makoshi, Jpn. J. Appl. Phys., Part 1 **35**, 3706 (1996).
[70] M. Stopa, Phys. Rev. Lett. **88**, 146802 (2002).